3D Holographic Imaging of Multi-Circular SAR Via Atomic Norm Minimization

1st Ang Ji
State Key Laboratory of Millimeter Waves
Southeast University
Nanjing, China
angji@seu.edu.cn

2nd Gang Xu
State Key Laboratory of Millimeter Waves
Southeast University
Nanjing, China
gangxu@seu.edu.cn

3rd Hongjun Wei
Shanghai Institute of Technical Physics of the Chinese Academy of Sciences
Shanghai, China
weihj@mail.sitp.ac.cn

4th Jialian Sheng
Shanghai Radio Equipment Research Institute
Shanghai, China
S.jialian@gmail.com

5th Wei Hong
State Key Laboratory of Millimeter Waves
Southeast University
Nanjing, China

2023 4th China International SAR Symposium (CISS) | 979-8-3503-0795-5/23/$31.00 ©2023 IEEE | DOI: 10.1109/CISS60136.2023.10379887

***Abstract*—Compared to multi-linear synthetic aperture radar (MLSAR), multi-circular SAR (MCSAR) can obtain (360°) high-resolution 3D images of the observed scenes. In this paper, a gridless compressive sensing method based on atomic norm minimization (ANM) is proposed for super-resolution holographic 3D imaging. The entire circle aperture data is divided into several subapertures, and then 3D imaging is performed independently. For all subapertures, the proposed method is utilized for tomographic domain imaging after 2D imaging and phase calibration. The final image is generated through the incoherent combination of subaperture 3D images. Finally, experiments with the GOTCHA dataset validate the effectiveness of the proposed method.**

***Index Terms*—Multi-circular SAR (MCSAR), atomic norm minimization (ANM), holographic SAR (HoloSAR).**

I. Introduction

3D synthetic aperture radar (SAR) imaging has great significance in millitary reconnaissance since it can provide 3D scattering properties of interested targets [1], [2]. As a special spotlight SAR imaging mode, circular SAR (CSAR) can demonstrate 3D reconstruction with full azimuth angle (360°). In theoy, single-flight CSAR has 3D imaging capability but its reconstruction results will be distorted by the undesirable sidelobes. SAR Tomography (TomoSAR) can form synthetic aperture in elevation through repeated linear trajectories, but it still encounters the limition of azimuth angle. Holographic SAR (HoloSAR) Tomography is the combination of CSAR and TomoSAR, multi-circular flights are repeated in different elevation to acquire echo data [3]. Considering cost control and difficulties of data acquisition, sparse and irregular evaluation sampling is unavoidable, which will reduce the quality of final 3D iamging results.

In the past years, some methods have been proposed to acquire high quality 3D reconstruction results. A Fourier-based method is used to focus in elevation dimension [4]. This method has high computational efficiency, yet it is susceptible to the influence of noise. The Iterative adaptive approach (IAA) can avoid spatial smoothing, but its iterations involve many matrix inversion calculations, which can introduce potential errors [5]. As a sparse reconstruction technique, compressed sensing (CS) has been widely applied in TomoSAR [6]- [8]. Nonetheless, the performance of CS depend on gird partition heavily, thus the off-grid CS via atomic norm minimization (ANM) may represent a more judicious alternative [9], [10].

In this paper, a tomographic 3D imaging method based on ANM has been proposed. The remainder of this paper is organized as follows. In section II, imaging geometry and signal model of HoloSAR are given. Section III describes the propoesd method based on ANM. Experiments results with real data are discussed in section IV to verify the effectiveness of propoesd method. Finally, section V provides the conclusion of this paper.

II. Signal Model

The data acquisition geometry of MCSAR is shown in Fig. 1. Airborne radar flies around the region of interest, forming a total of M circular trajectories at different heights. Since the backscattering properties of most targets are anisotropic, the incoherent imaging is adopted in this article. We divide a complete circular aperture into N nonoverlapping subapertures (SA-$n, n = 1, 2, ..., N$), and the azimuth angle extent of each subaperture is $\Delta\theta$, i.e., $N \times \Delta\theta = 360^\circ$. The proposed 3D imaging method is performed in each subapertures, and all 3D imaging results are combined incoherently in the same Cartesian coordinate system to produce final 3D image.

Fig. 2 demonstrates the holographic processing for full aperture MCSAR data. For SA-n, M single look complex

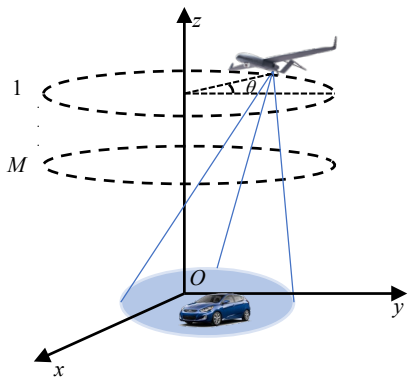

Fig. 1. Data acquisition geometry of MCSAR.

(SLC) images can be obtained after phase calibration. The complex value g_m of certain pixel can be expressed as

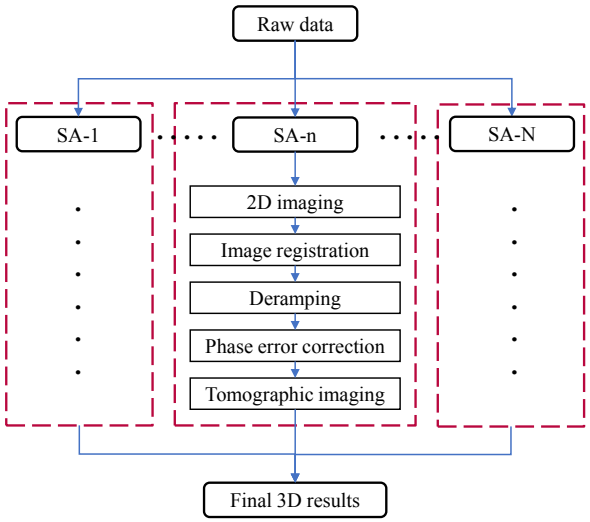

Fig. 2. Framework of 3D holographic imaging.

$$g_m = \int \gamma(s)\, exp(j2\pi\xi_m s)ds \tag{1}$$

where $m = 1, 2, ..., M$ is the index of pass, $\gamma(s)$ denotes the reflectivity function along tomographic coordinate s, and $\xi_m = 2b_m/(\lambda r)$ is the spatial frequency, which respect to baseline b_m, center wavelength λ and range r.

As described in (1), g_m and $\gamma(s)$ form Fourier transform pairs, thus the tomographic focus results can be obtained by performing IFFT$[\cdot]$ to g_m:

$$\gamma(s) = IFFT[g_m] \tag{2}$$

Although Fourier-based method has high computational efficiency, the imaging results are significantly affected by irregular baselines. The performance can be improved using non-uniform Fourier transform, but is still susceptible to noise.

Discretizing the model in (1), the discrete-space model can be expressed as

$$\boldsymbol{g} = \boldsymbol{\Phi}\boldsymbol{\gamma} + \boldsymbol{\varepsilon} \tag{3}$$

where $\boldsymbol{g} = [g_1, g_2, \cdots, g_M]^T$ is an $M \times 1$ observation vector. $\boldsymbol{\Phi} = [\boldsymbol{\phi}_1, \boldsymbol{\phi}_2, \cdots, \boldsymbol{\phi}_L]$ is an $M \times L$ observation matrix with $\boldsymbol{\phi}_l = \left[e^{j2\pi\xi_1 s_l}, e^{j2\pi\xi_2 s_l}, \cdots, e^{j2\pi\xi_M s_l}\right]^T$. $\boldsymbol{\gamma} = [\gamma(s_1), \gamma(s_2), \cdots, \gamma(s_L)]^T$ is an $L \times 1$ scatter coefficient vector. $\boldsymbol{\varepsilon}$ is an $M \times 1$ noise vector.

III. Tomographic Imaging via Atomic Norm Minimization

In Fig. 2, 3D holographic imaging can be implemented as a "2D+1D" manner for SA-n. Therefore, the 3^{rd} dimension(i.e., tomographic dimension) imaging of SA-n is performed per pixel independently. For every pixel in 2D SLC images, it is assumed that there are K strong catters in one pixel :

$$\boldsymbol{g}(p) = \sum_{k=1}^{K} \boldsymbol{\phi}_k \gamma_k + \varepsilon = \boldsymbol{\Phi}\boldsymbol{\gamma} + \varepsilon \tag{4}$$

where $p = 1, 2, ..., P$ is the index of pixels, P is number of pxiels corresponding to SA-n.

The $\boldsymbol{\Phi}$ can be treated as a combination of atom series with the atomic set defined as

$$\mathcal{A} = \{\boldsymbol{\phi}_k(s_k) \mid s_k \in \mathbb{R}\} \tag{5}$$

The atomic norm of $\boldsymbol{g}(p)$ is

$$\|\boldsymbol{g}(p)\|_{\mathcal{A}} = \inf\left\{\sum_k \gamma_k : \boldsymbol{g}(p) = \sum_k \boldsymbol{\phi}_k\gamma_k, \gamma_k > 0, \boldsymbol{\phi}_k \in \mathcal{A}\right\} \tag{6}$$

The atomic soft thresholding (AST) method can be used to eliminate the influence of noise and estimate the covariance matrix

$$\min_{\tilde{\boldsymbol{g}}} \|\tilde{\boldsymbol{g}}\|_{\mathcal{A}} \quad \text{s.t. } \|\tilde{\boldsymbol{g}} - \boldsymbol{g}\|_2^2 \le \sigma \tag{7}$$

where σ is noise variance of noise ϵ.

The atomic norm $\|\tilde{\boldsymbol{g}}\|_{\mathcal{A}}$ can be solved via semidefinite programming (SDP) as

$$\|\tilde{\boldsymbol{g}}\|_{\mathcal{A}} = \min_{\rho,\boldsymbol{u}} \frac{1}{2}(\rho + u_1) \quad \text{s.t.} \begin{bmatrix} \rho & \tilde{\boldsymbol{g}}^H \\ \tilde{\boldsymbol{g}} & T(\boldsymbol{u}) \end{bmatrix} \ge \mathbf{0} \tag{8}$$

where $\boldsymbol{u}$ is an $M \times 1$ vector and its corresponding Toeplitz matrix is $T(\boldsymbol{u})$.

Thus, (7) could be written as

$$\min_{\rho,\boldsymbol{u},\tilde{\boldsymbol{g}}} \frac{\mu}{2}(\rho + u_1) + \frac{1}{2}\|\tilde{\boldsymbol{g}} - \boldsymbol{g}\|_2^2 \quad \text{s.t.} \begin{bmatrix} \rho & \tilde{\boldsymbol{g}}^H \\ \tilde{\boldsymbol{g}} & T(\boldsymbol{u}) \end{bmatrix} \ge \mathbf{0} \tag{9}$$

where $T(\boldsymbol{u})$ is the denoising estimate of the covariance matrix. Since $T(\boldsymbol{u})$ is given, $\boldsymbol{\phi}_k$ can be obtained via MUSIC algorithm.

IV. Experiments

In this section, we use the GOTCHA dataset to verify the effectiveness of the propoesd method. This dataset is released by the Air Force Research Laboratory (AFRL) [11], and it consists of 8 pass radar measurement data at X-band with full polarization.

A. 2D Imaging

As shown in Fig. 3, the trajectory of airborne radar is not an ideal circle due to various factors in the process of data acquisition.

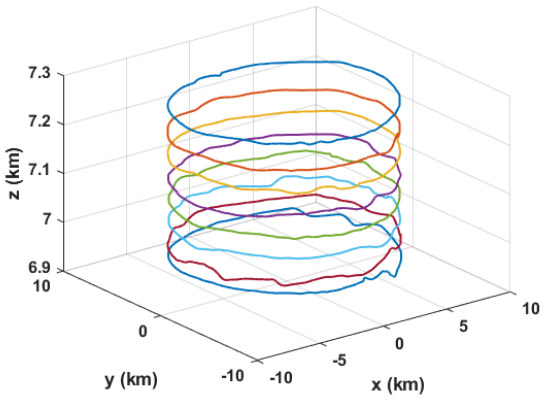

Fig. 3. Actual trajectories in the GOTCHA dataset.

Full azimuth pass 1^{st} data with HH polarization is imaged using BP algorithm [12] to to compare azimuthal coherent imaging with incoherent imaging in CSAR mode. 2D SAR images are shown in Fig. 4 and the range of magnitude display is $[-35\ 0]$ dB. It can be found that compared to coherent imaging in Fig. 4(a), incoherent process can obtain results with higher singnal-to-noise (SNR) and clearer contours of targets (vehicles, etc).

B. 3D Holographic Imaging

In Fig. 4, there are many vehicles in the imaging scene. We select regions where a Ford Taurus wagon is located to validate the effectiveness of the propoesd method described in section III. The entire circular is uniformly divided into 72 nonoverlapping subapertures, each with an azimuth angle extent of $5°$. The BP algorithm is utilized to generate SLC 2D images, and then a phase calibration method based on Phase Gradient Autofocus (PGA) is performed [13]. The 3D holographic results are shown in Fig. 5 and the color is the mapping of the height of reconstructed vehicle in the images. The size and structure of reconstructed vehicle is basically consist with the actual size of the Ford Taurus, which verifies the effectiveness of proposed method. As a comparison, the result of non-uniform Fourier method is also presented in Fig. 5, but the image of propoesd method has a clearer vehicle contour. In order to have a better comparison, three different views of imaging results are also demonstrated in Fig. 6. The range of magnitude display is [-25 0] dB.

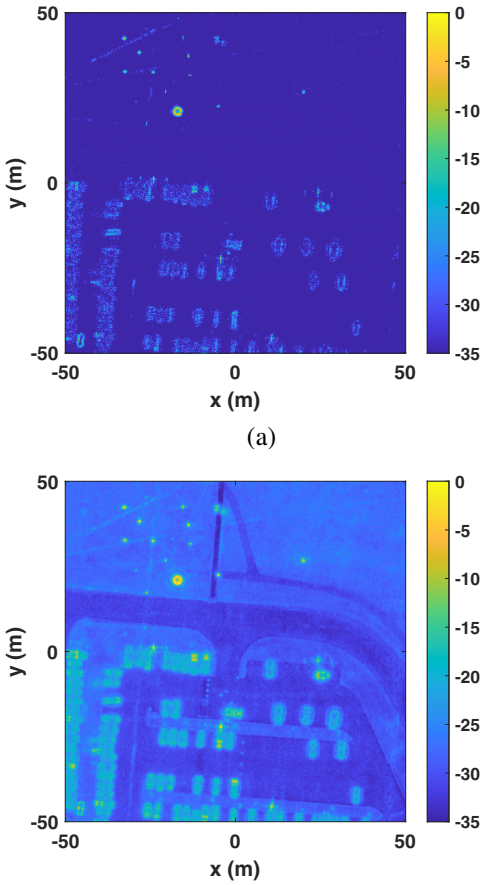

Fig. 4. 2D SAR image of azimuthal coherent imaging and incoherent imaging. (a) Coherent imaging. (b) Incoherent imaging.

V. Conclusion

In this paper, a MCSAR 3D imaging method based on atomic norm minimization is proposed. The entire circular are divided into several nonoverlapping subapertures firstly. For each subaperture, following a sequence of steps including 2D imaging, deramping, image registration, and phase error correction, the proposed method is performed for tomographic dimension imaging. Finally, the ultimate HoloSAR 3D image can be achieved through incoherent combination of images of subapertures. The effectiveness of proposed method is validated through experiments with the GOTCHA dataset.

Acknowledgment

The authors would like to thank the Air Force Research Laboratory (AFRL) for providing the valuable GOTCHA dataset.

This work was supported by the National Natural Science Foundation of China (NSFC) under Grant 62071113, in part by the Natural Science Foundation of Jiangsu Province under Grant BK20211559, in part by the Fundamental Research Funds for the Central Universities under Grant 2242022k60008.

(a)

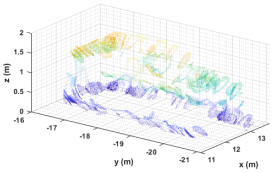

(b)

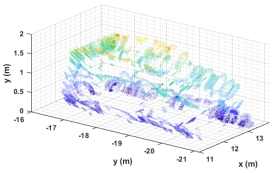

(c)

Fig. 5. Optical and 3D reconstruction image of Ford Taurus. (a) Optical image. (b) Proposed method. (c) Non-uniform Fourier method.

REFERENCES

[1] A. Moreira, P. Prats-Iraola, M. Younis, G. Krieger, I. Hajnsek and K. P. Papathanassiou, "A tutorial on synthetic aperture radar", IEEE Geosci. Remote Sens. Mag., vol. 1, no. 1, pp. 6-43, Mar. 2013.

[2] B. Zhang, G. Xu, H. Yu, H. Wang, H. Pei and W. Hong, "Array 3-D SAR tomography using robust gridless compressed sensing", IEEE Trans. Geosci. Remote Sens., vol. 61, 2023.

[3] Q. Bao, Y. Lin, W. Hong, W. Shen, Y. Zhao and X. Peng, "Holographic SAR tomography image reconstruction by combination of adaptive imaging and sparse Bayesian inference", IEEE Geosci. Remote Sens. Lett., vol. 14, no. 8, pp. 1248-1252, Aug. 2017.

[4] A. Reigber and A. Moreira, "First demonstration of airborne SAR tomography using multibaseline L-band data", IEEE Trans. Geosci. Remote Sens., vol. 38, no. 5, pp. 2142-2152, Sep. 2000.

[5] W. Sun, H. C. So, Y. Chen, L.-T. Huang, and L. Huang, "Approximate subspace-based iterative adaptive approach for fast two-dimensional spectral estimation," IEEE Trans. Signal Process, vol. 62, no. 12, pp. 3220–3231, Jun. 2014

[6] X. Zhu and R. Bamler, " Tomographic SAR inversion by L 1 -norm regularization—The compressive sensing approach ", IEEE Trans. Geosci. Remote Sens., vol. 48, no. 10, pp. 3839-3846, Oct. 2010.

[7] A. Budillon, A. Evangelista and G. Schirinzi, "Three-dimensional SAR focusing from multipass signals using compressive sampling", IEEE Trans. Geosci. Remote Sens., vol. 49, no. 1, pp. 488-499, Jan. 2011.

[8] X. X. Zhu and R. Bamler, "Super-resolution power and robustness of compressive sensing for spectral estimation with application to spaceborne tomographic SAR", IEEE Trans. Geosci. Remote Sens., vol. 50, no. 1, pp. 247-258, Jan. 2012.

[9] Z. Yang and L. Xie, "On gridless sparse methods for line spectral estimation from complete and incomplete data", IEEE Trans. Signal Process., vol. 63, no. 12, pp. 3139-3153, Jun. 2015.

[10] Z. Yang and L. Xie, "Exact joint sparse frequency recovery via optimization methods", IEEE Trans. Signal Process., vol. 64, no. 19, pp. 5145-5157, Oct. 2016.

[11] C. H. Casteel, L. A. Gorham, M. J. Minardi, S. M. Scarborough, K. D. Naidu and U. K. Majumder, "A challenge problem for 2D/3D imaging of targets from a volumetric data set in an urban environment", Proc. SPIE 14th Algorithms Synth. Aperture Radar Imag. Int. Soc. Opt. Photon., vol. 6568, pp. 97-103, Eds. 2007.

[12] B. Zhang, G. Xu, R. Zhou, H. Zhang and W. Hong, "Multi-channel back-projection algorithm for mmWave automotive MIMO SAR imaging with Doppler-division multiplexing", IEEE J. Sel. Topics Signal Process., Sep. 2022.

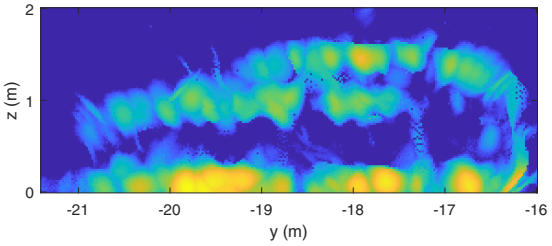

(a)

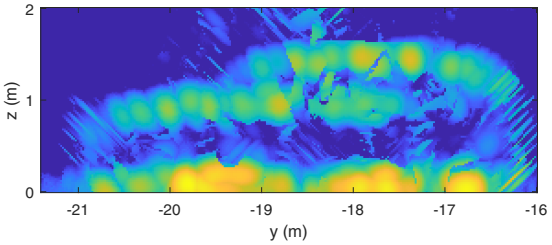

(b)

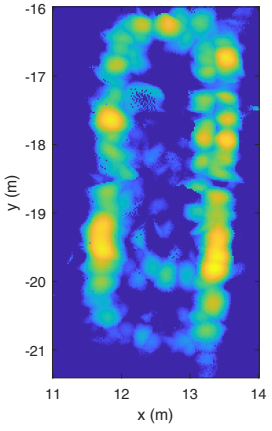

(c)

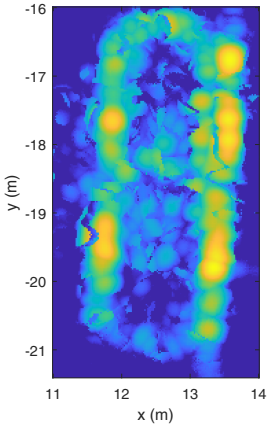

(d)

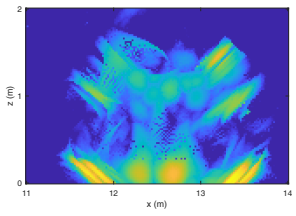

(e)

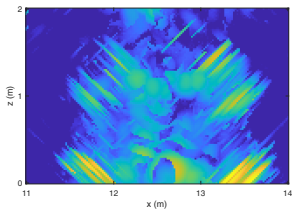

(f)

Fig. 6. Different views of 3D reconstruction results ((a)(c)(e) propoesd method, (b)(d)(f) Non-uniform Fourier method). (a) and (b) View of YOZ. (c) and (d) View of XOY. (e) and (f) View of XOZ.

[13] D. Feng, D. An, L. Chen and X. Huang, "Holographic SAR tomography 3-D reconstruction based on iterative adaptive approach and generalized likelihood ratio test", IEEE Trans. Geosci. Remote Sens., vol. 59, no. 1, pp. 305-315, Jan. 2021.